Destabilization of DNA through interstrand crosslinking by UO22+

Rossberg, A.; Abe, T.; Okuwaki, K.; Barkleit, A.; Fukuzawa, K.; Nakano, T.; Mochizuki, Y.; Tsushima, S.;

Originally published:

January 2019

Chemical Communications 55(2019), 2015-2018

DOI: https://doi.org/10.1039/C8CC09329F

DNA destabilization by uranium binding

*André Rossberg [1], Takaya Abe [2], Koji Okuwaki [2], Astrid Barkleit [1], Kaori Fukuzawa [3], Tatsuya Nakano,[4] Yuji Mochizuki [2,5], and Satoru Tsushima [1,6] **

1 Institute of Resource Ecology, Helmholtz–Zentrum Dresden–Rossendorf (HZDR), Dresden, 01328, Germany.

2 Department of Chemistry and Research Center for Smart Molecules, Rikkyo University, Tokyo, 171–8501, Japan.

3 Department of Physical Chemistry, Hoshi University, Tokyo, 142–8501, Japan.

4 Division of Medicinal Safety Science, National Institute of Health Sciences, Kawasaki, 210-9501, Japan.

5 Institute of Industrial Science, The University of Tokyo, Tokyo, 153–8505, Japan.

6 Tokyo Tech World Research Hub Initiative (WRHI), Institute of Innovative Research, Tokyo Institute of Technology, Tokyo, 152–8550, Japan.

AUTHOR INFORMATION

Corresponding Author

*E-mail: S.Tsushima@hzdr.de

ABSTRACT: UO_2^{2+} exhibits high affinity towards DNA causing genotoxic effect. There is increased phenomenological understanding about uranium genotoxicity, whereas little is known about U–DNA interaction at a molecular level. X–ray absorption spectroscopic (XAS) measurement of the U–DNA adduct revealed predominance of 1:1 coordination of UO_2^{2+} to the backbone phosphate with minor contribution from crosslinking UO_2^{2+} which bridges phosphates from two different strands. The structures obtained by classical molecular dynamics simulation of the system containing UO_2^{2+} and Dickerson–Drew dodecamer are in line with the conformations deduced from XAS. We focused on the U–DNA crosslinking structure and analysed the effect of UO_2^{2+} binding to DNA using fragment molecular orbital method. The binding of UO_2^{2+} hardly affects hydrogen bonds between nucleobase pairs whereas it destabilizes the π–π stacking between the two nucleobases in the vicinity of UO_2^{2+}–bound phosphate. Thereby, fragility of DNA backbone increases upon UO_2^{2+} binding.

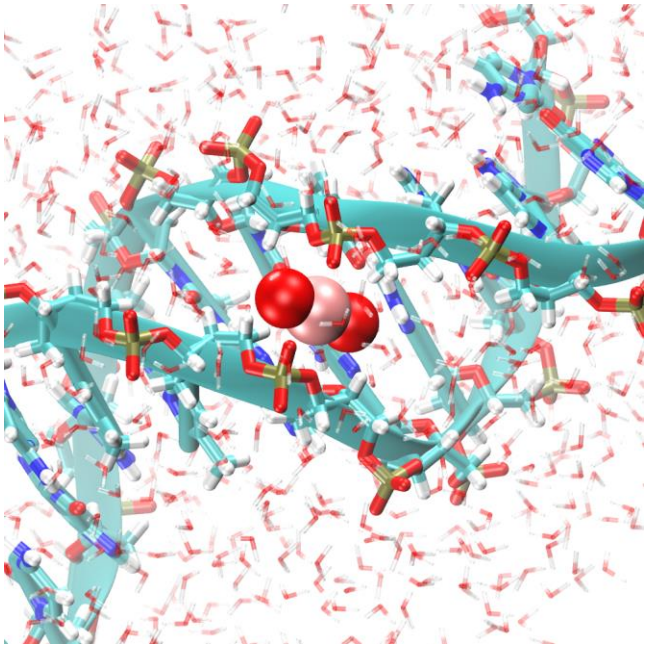

KEYWORDS. Fragment molecular orbital method, chemotoxicity, uranyl(VI), interstrand crosslink, EXAFS.

Uranium is weakly radioactive thereby causing toxicity towards organism through radiation and radiolysis. Alpha particle can cause direct deoxyribonucleic acid (DNA) damage whereas radiolysis of water induces chemotoxicity *via* H_2O_2 production. These effects, however, remain overall modest because of the long half–lives of naturally abundant uranium isotopes (>10^8 years) and also because under the pH–Eh conditions where most organisms are concerned uranium are not highly soluble. Only under extreme circumstances, such as in mine drainage or at heavily contaminated sites from the nuclear legacy, uranium radiotoxicity becomes real threat to living organisms.[1]

Apart from radiological issues, uranium causes chemotoxicity. Use of depleted uranium in the Gulf War and in Kosovo spawned heated discussions on U genotoxicity including *in vitro* carcinogenic studies where cytotoxic effect of U was associated not with its radioactivity but ascribed to U being heavy element.[2] *In vivo* studies using rats showed U accumulation in kidney and bones [3] as well as causing stress to their immune system [4] when U concentration exceeded certain threshold. Various biophysical studies focused on U interaction with metalloproteins (e.g. transferrin, albumin) because of their high affinity.[5,6] However, *in vivo* studies showed minor increase of U in serum due to its easy urinary excretion. U–protein interaction is apparently not the major pathway which associates with U genotoxicity. Uranium–DNA binding has not been the focus of mutagenic and cytotoxic studies as this reaction was believed to be only relevant in connection with extracellular reaction such as biomineralization of U or photo–induced cleavage of U–DNA adduct.[7-11] Recently it was demonstrated that direct exposure of mammalian cell to U can lead to formation of U–DNA adduct at high loading level.[12] On the other hand, various genotoxicity of U are known such as mutagenicity,[12,13] aneugenicity,[14] cytotoxicity,[15]

clastogenicity,[16] and tumorigenicity,[17] which can cause DNA strand break as well as chromosome aberrations. DNA strand break occurs when replication fork encounters DNA lesions such as abasic site, mismatch, or interstrand crosslink.

UO_2^{2+} binds to DNA presumably through phosphate group of its sugar–phosphate backbone. This, however, has never been confirmed *via* direct spectroscopic measurement. We prepared samples containing UO_2^{2+} (1–5 mM) and genomic DNA from salmon testes keeping the PO_4/U ratio between 4 and 5 at pH 5.9–6.3 (SI). The U L_{III}–edge extended X–ray absorption fine structure (EXAFS) spectra were measured at the Rossendorf Beamline (BM20) [18] at the European Synchrotron (ESRF), Grenoble, France (SI). To avoid photodegradation, the samples were kept in dark. Beside the EXAFS spectra of UO_2^{2+} with DNA, we also measured UO_2^{2+}–bound sugar phosphates (glucose and fructose phosphates), aqueous U(VI) hydrate ($UO_2(H_2O)_5^{2+}$) and the hydrated calcium uranyl phosphate mineral meta–autunite as references (Fig. 1). The sample list is given in Table S1. Overall similarity in the EXAFS spectra was observed among the local environment around U in U–DNA and those in U–sugar phosphates or in meta–autunite supporting UO_2^{2+} binding to DNA through the phosphate group (Fig. 1). For a quantitative analysis of the coordination number of PO_4 ($CN_{phosphate}$) and H_2O (CN_{water}) we performed iterative target transformation factor analysis (ITFA) [19] on the EXAFS spectra (SI), while a EXAFS spectral series of U(VI) complexes with glucose–1–phosphate served as a measure of the reliability of our analysis strategy (SI). The ITFA spectral decomposition yielded two spectral components which enable reproduction of all spectra by their linear combination (Fig. S3 and S5). The components are the EXAFS signals of one monodentately coordinated phosphate group and one coordinated water molecule, hence both components are present in the reference spectra of meta–autunite and U(VI) hydrate (Fig. S1and S2). Since for the two

references $CN_{phosphate}$ and CN_{water} are known these values were used as a constraint for ITFA in order to determine $CN_{phosphate}$ and CN_{water} for all U-DNA and U–sugar phosphate samples (Fig. S4, Table S5).

In the U–sugar phosphates, formation of both 1:1 and 1:2 complexes are confirmed by observing an average $CN_{phosphate}$ of 1.0 to 2.2, being consistent with our previous EXAFS study on U–sugar phosphates.[20] For U–DNA, $CN_{phosphate}$ was found to be between 0.9 and 1.5. It appears clear that a part of U has more than one PO_4 coordinated. Steric effect hinders one UO_2^{2+} to bind simultaneously to two separate DNA so that $CN_{phosphate} > 1.0$ implies that UO_2^{2+} partially binds to two phosphate groups within the same DNA presumably *via* interstrand crosslink. Formation of interstrand link by UO_2^{2+} has been reported earlier.[7,21] Such link can block replication of DNA and may potentially cause critical genotoxic impact. We are therefore interested in understanding the effect of UO_2^{2+} bridging to DNA in a molecular level.

We performed classical molecular dynamics (MD) simulations and analyzed the binding behavior of UO_2^{2+} to Dickerson–Drew B–DNA dodecamer (DDD, d[CGCGAATTCGCG]$_2$). Assuming that UO_2^{2+} is bound to at least one phosphate group of DDD, we calculated using two different initial structures; (**A**) UO_2^{2+} bound to the phosphate between two deoxyriboses proximal to 9C and to 10G, (**B**) UO_2^{2+} bound to the phosphate between two deoxyriboses proximal to 6'T and to 7'A. We performed 150 ns MD simulation for **A** and **B**. For simulation **A**, UO_2^{2+} remained steadily bound to the same phosphate during the entire simulation and there was no sign of UO_2^{2+} interacting with other phosphate (**Fig. S6**). For simulation **B**, after about 20 ns simulation time, UO_2^{2+} started to interact with the other strand across the minor groove and eventually gets stably bound to the phosphate of the opposite strand between two deoxyriboses proximal to 9C and to 10G. However, UO_2^{2+} still remained steadily bound to the original host

phosphate thus forming an interstrand crosslink between the two strands across the minor groove of DDD. Once an interstrand link is formed, it remained stable until the end of the simulation (150 ns). In **Fig. 2A**, the structures from the MD trajectory at each 1 ns between 50 to 150 ns simulation time are superimposed. The O_{pho}–U–O_{pho} unit remained rigid whereas the UO_2^{2+} unit can freely rotate along the O_{pho}–U–O_{pho} axis accompanied by water exchange of UO_2^{2+}. To further explore the local structure around UO_2^{2+}, a MD snapshot at t = 150 ns is given in **Fig. 2B**. Two phosphates which are bridged by UO_2^{2+} have two hanging oxygens – one pointing to the minor groove and other to the major groove. Since these two oxygens are mutually exclusive and do not exchange during the entire simulation time, in order to have UO_2^{2+} interact with the opposite strand, it was mandatory to have UO_2^{2+} bound to the oxygen in the minor groove. This situation made the difference between simulation **A** and **B** – former having UO_2^{2+} attached to the oxygen in the major groove, thereby was unable to interact with phosphate from the opposite strand. Finally, in **Fig. 2C**, the local structure around the first coordination shell of UO_2^{2+} and the interatomic distances are given. Despite that the force field parameters of UO_2^{2+} are developed only to reproduce its interaction with waters, in the MD simulation of U–DNA, the UO_2^{2+}–phosphate interaction is well–reproduced in terms of bond lengths and coordination numbers. Besides, the global conformation of the U–DNA showing possible formation of interstrand crosslink is also consistent with earlier studies [7,21] and also with our EXAFS results. Interstrand crosslink by metal ion(s) across the minor groove of DNA has been previously confirmed for alkaline, alkaline–earth, and transition metal cations in the form of two hexaaquo complexes bridging between the two strands through electrostatic interactions. [22,23] The bridging *via* double $[M(H_2O)_6]^{2+}$ complexes is somewhat different from the case of UO_2^{2+} in which single UO_2^{2+} forms strong inner–sphere complex through PO_4–U–PO_4 network formation. Therefore, although

metal ion binding to phosphate is generally thought to stabilize DNA,[23] it remains an open question if the same rule applies to UO_2^{2+} binding to DNA.

Since we have now a molecular picture of interstrand crosslinking of UO_2^{2+}–bound DDD, we focus on the effect of UO_2^{2+} binding to the backbone of DDD at quantum chemical level in the framework of fragment molecular orbital method (FMO). In FMO,[24] the molecular system of interest is divided into small fragments, and each fragment and fragment pair is subjected to self–consistent field (SCF) calculations and successive second–order Møller–Plesset perturbation theory (MP2) calculations.[25] Electronic structure of the whole system is then reconstituted. This procedure drastically reduces computational costs allowing to study the full protein or DNA at MP2 level.[26] By combining FMO with MD, we are able to compensate some of the issues associated with the use of classical MD, and can more accurately assess energetics involving weak interactions such as H–bonds and π–π stacking. In **Fig. 3**, we show inter–fragment interaction energy (IFIE) between the base pairs (H–bonds) and between the neighboring bases (π–π stacking). These are average values obtained from 100 MD snapshots and standard deviations are given in a separate figure (**Fig. S4**). The IFIEs were calculated in the absence and in the presence of UO_2^{2+} in order to quantify the effect of UO_2^{2+} binding. It appears clear that H–bonds between the bases (horizontal arrows in **Fig. 3**) are hardly affected by the presence of UO_2^{2+} and that the H–bonds between the base pairs remain stable upon UO_2^{2+} binding. By contrast, base stacking interaction are clearly affected by UO_2^{2+} binding. As shown in **Fig. 3**, UO_2^{2+} is bound to the phosphates between 9C and 10G. The 9C–10G stacking interaction gets stabilized upon UO_2^{2+} binding whereas those between the neighboring bases, namely 8T–9C and 10G–11C, get destabilized. The 9C–10G stacking distance shortens upon UO_2^{2+} binding from 4.38 ± 0.51 to 3.97 ± 0.23 Å (and the standard deviation of the stacking energy drops almost to

the half correspondingly (**Fig. S7**)) whereas for the 8T–9C and 10G–11C it is elongated by 0.29 and 0.38 Å, respectively. The same UO_2^{2+} is bound to the phosphate between 6'T and 7'A. UO_2^{2+} binding slightly strengthen the 6'T–7'A stacking and also that between the neighboring bases. However, the effect is overall weak compared to binding to the 9C–10G. It appears that UO_2^{2+} binding has larger effect to CG pairs when compared to AT pairs presumably because of guanine (G) being the most redox–sensitive nucleobase. In order to have more global view of the effect of UO_2^{2+} binding, the sum of stacking and H–bond energy within DDD were calculated, which are -710.1 ± 22.1 and -703.3 ± 24.2 kcal/mol without and with UO_2^{2+}, respectively. From the comparison of these two numbers, the effect of UO_2^{2+} binding appears to be subtle. However, when we plot distribution of sum of the energy from 100 MD snapshots instead of taking an average (**Fig. S8**), we see difference in their distribution suggesting a loss of overall stability of DNA upon UO_2^{2+} binding. Most importantly, if stacking interaction gets locally destabilized, it may induces fragile part in DNA and can eventually contribute to destabilization of DNA.

To summarize, X–ray absorption study of U–DNA suggested predominance of one–to-one coordination of UO_2^{2+} and PO_4^- group. But there is also evidence suggesting the presence of the species with 2 PO_4^- bound to UO_2^{2+} suggesting an interstrand crosslink within the DNA. Combined MD-FMO study on DNA with and without UO_2^{2+} showed that interstrand crosslink can slightly destabilize stacking interaction between the nucleobases proximal to the UO_2^{2+} bound phosphate. This might be a clue for genotoxicity of uranium and further study in this direction is worthwhile.

ASSOCIATED CONTENT

Supporting Information. The Supporting Information is available free of charge on the ACS Publications website at DOI:10.1021/acs.jpclett.XXXXXXX

Sample preparation and sample list for EXAFS. Details of EXAFS measurements and factor analysis (ITFA). Computational (MD, FMO) details. MD snapshots of UO_2^{2+}–bound DNA without interstrand crosslink. Inter-fragment interaction energy of DNA with/without UO_2^{2+} and standard deviations. (PDF)

AUTHOR INFORMATION

ORCID

Astrid Barkleit: 0000-0003-3241-3443

Kaori Fukuzawa: 0000-0001-5357-8250

Yuji Mochizuki: 0000-0002-7310-5183

Satoru Tsushima: 0000-0002-4520-6147

Notes

The authors declare no competing financial interests.

ACKNOWLEDGMENT

This work was partially funded by the Ministry of Education, Culture, Sports, Science, and Technology of Japan (MEXT) under the framework "Grant–in–Aid for Scientific Research B" (16H04635). MEXT also supported this project as a Social and Scientific Priority Issue 6 (Accelerated Development of Innovative Clean Energy Systems) for the post–K supercomputing facility of Japan (FS2020). We thank A.C.Scheinost, J.Raff, K. Takao, Y.Komeiji, E.Miyoshi, and K.Fahmy for stimulating discussions.

REFERENCES

(1) Priest, N.D. Toxicity of depleted uranium. *Lancet,* **2001**, *357*, 244–246.

(2) Domingo, J.L. Reproductive and developmental toxicity of natural and depleted uranium: a review. *Reprod. Toxicol*. **2001**, *15*, 603–609.

(3) Zhu, G., Tan, M., Li, Y., Xiang, X. Hu, H., Zhao, S. Accumulation and Distribution of Uranium in Rats after Implantation with Depleted Uranium Fragments. *J. Radiat. Res.* **2009**, *50*, 183–192.

(4) Dublineau, I. Grison, S., Linard, C., Baudelin, C., Dudoignon, N., Souidi, M., Marquette, C., Paquet, F., Aigueperse, J., Gourmelon, P. Short-term effects of depleted uranium on immune status in rat intestine. *J. Toxicol. Environ. Health A*, **2006**, *69*, 1613–1628.

(5) Vidaud, C., Dedieu, A., Basset, C., Plantevin, S., Dany, I., Pible, O., Quéménur, E. Screening of Human Serum Proteins for Uranium Binding. *Chem. Res. Toxicol.* **2005**, *18*, 946–953.

(6) Montavon, G., Apostolidis, C., Bruchertseifer, F., Repinc, U, Morgenstern, A. Spectroscopic study of the interaction of U(VI) with transferrin and albumin for speciation of U(VI) under blood serum conditions, *J. Inorg. Biochem*. **2009**, *103*, 1609–1616.

(7) Nielsen, P.E., Hiort, C., Sönnichsen, S.H., Buchardt, O., Dahl, O., Nordèn, B. DNA Binding and Photocleavage by Uranyl(VI) (UO_2^{2+}) Salts. *J. Am. Chem. Soc.* **1992**, *114*, 4967–4975.

(8) Nielsen, P.E. Uranyl footprinting. *Methods Mol. Biol.* **2009***, 543*, 87–96.

(9) George, S.A., Whittaker, A.M., Stearns, D.M. Photoactivated Uranyl Ion Produces Single Strand Breaks in Plasmid DNA. *Chem. Res. Toxicol*. **2011**, *24*, 1830–1832.

(10) Lindemose, S., Nielsen, P.E., Hansen, M. Møllegaard, N.E. A DNA minor groove electronegative potential genome map based on photo-chemical probing. *Nucl. Acids Res*. **2011**, *39*, 6269–6276.

(11) Cepeda-Plaza, M., Null, E.L., Lu, Y. Metal ion as both a cofactor and a probe of metal-binding sites in a uranyl-specific DNAzyme: a uranyl photocleavage study. *Nucl. Acids Res*. **2013**, *41*, 9361–9370.

(12) Stearns, D.M., Yazzie, M., Bradley, A.S., Coryell, V.H., Shelley, J.T., Ashby, A., Asplund, C.S., Lantz, R.C. Uranyl acetate induces hprt mutations and uranium–DNA adducts in Chinese hamster ovary EM9 cells. *Mutagenesis*, **2005**, *6*, 417–423.

(13) Miller, A.C., Fuciarelli, A.F., Jackson, W.E., Ejnik, E.J., Emond, C., Strocko, S., Hogan, J., Page, N., Pellmar, T. Urinary and serum mutagenicity studies with rats implanted with depleted uranium or tantalum pellets. *Mutagenesis*, **1998**, *13*, 643–648.

(14) Darolles, C., Broggio, D., Feugier, A., Frelon, S., Dublineau, I., De Meo, M., Petitot, F. Different genotoxic profiles between depleted and enriched uranium. *Toxicol. Lett.* **2010***, 192*, 337–348.

(15) Wilson, J., Zuniga, M.C., Yazzie, F., Stearns, D.M. Synergistic cytotoxicity and DNA strand breaks in cells and plasmid DNA exposed to uranyl acetate and ultraviolet radiation. *J.Appl. Toxicol*. **2015**, *35*, 338–349.

(16) Wise, S.S., Thompson, W.D., Aboueissa, A., Mason, M.D., Wise, J.P. Particulate Depleted Uranium Is Cytotoxic and Clastogenic to Human Lung Cells. *Chem. Res. Toxicol*. **2007**, *20*, 815–820.

(17) Hahn, F.F., Guilmette, R.A., Hoover, M.D. Implanted depleted uranium fragments cause soft tissue sarcomas in the muscles of rats. *Environ. Health Perspect.* **2002**, *110*, 51–59.

(18) Reich, T., Bernhard, G., Geipel, G., Funke, H., Hennig, C., Rossberg, A., Matz, W., Schell, N., Nitsche, H. *Radiochim. Acta* **2000**, 88, 633-637.

(19) Rossberg, A., Reich, T., Bernhard, G. *Anal. Bioanal. Chem*. **2003**, 376, 631-638.

(20) Koban, A., Geipel, G., Roßberg, A., Bernhard, G. Uranium(VI) complexes with sugar phosphates in aqueous solution. *Radiochim. Acta* **2004**, 92, 903-908.

(21) Cepeda-Plaza, M., Null, E.L., Lu, Y. Metal ion as both a cofactor and a probe of metal-binding sites in a uranyl-specific DNAzyme: a uranyl photocleavage study. *Nucl. Acids Res.* **2013**, 41, 9361–9370.

(22) Egil, M. DNA-Cation Interactions: Quo Vadis? *Chem. Bio.* **2002**, 9, 277–286.

(23) Theophanides, T. , Anastassopoulou, J. The effects of metal ion contaminants on the double stranded DNA helix and diseases. *J. Environ. Sci. Health, A*. **2017**, 52, 1030–1040.

(24) Kitaura, K.; Asada, T.; Nakano, T.; Uebayashi, M. Fragment molecular orbital method: an approximate computational method for large molecules. *Chem. Phys. Lett.* **1999**, 313, 701–706.

(25) (a) Fedorov, D.G.; Nagata, T.; Kitaura, K. Exploring chemistry with the fragment molecular orbital method. *Phys. Chem. Chem. Phys.* **2012**, 14, 7562–7577. (b) Tanaka, S.; Mochuzuki, Y.; Komeiji, Y.; Okiyama, Y.; Fukuzawa, K. Electron-correlated fragment-molecular-orbital calculations for biomolecular and nano systems. *Phys. Chem. Chem. Phys.* **2014**, 16, 10310–10344.

(26) Fukuzawa, K.; Kurisaki, I.; Watanabe, C.; Okiyama, Y.; Mochizuki, Y.; Tanaka, S.; Komeiji, Y. Explicit solvation modulates intra- and inter-molecular interactions within DNA: Electronic aspects revealed by the *ab initio* fragment molecular orbital (FMO) method. *Comp. Theor. Chem.* **2015**, 1054, 29–37.

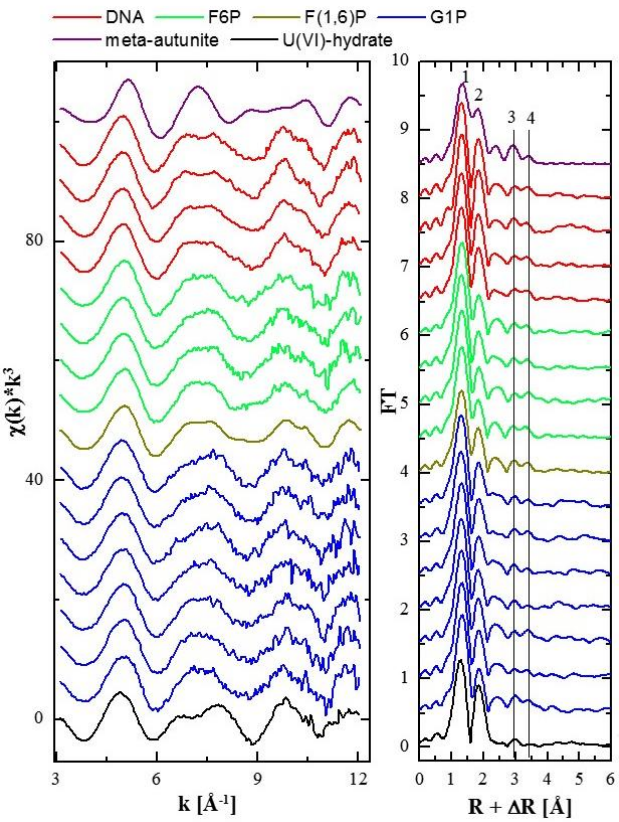

Figure 1. k^3-weighted U L_{III}-edge EXAFS spectra (left) and corresponding Fourier transform (right) of UO_2^{2+}–DNA samples, meta-autunite, U(VI)-hydrate and those of UO_2^{2+} with the sugar phosphates: fructose-(1,6)-diphosphate (F(1,6)P), fructose-6-phosphate (F6P) and glucose-1-phosphate (G1P). Labeled spectral features are explained in SI.

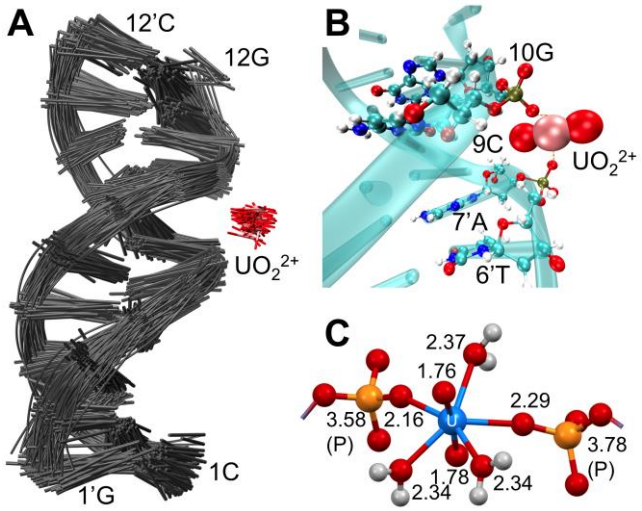

Figure 2. Room–temperature classical molecular dynamics (MD) simulations of the d[CGCGAATTCGCG]$_2$ (DDD) bound UO_2^{2+}. (**A**) Superimposed MD snapshots of UO_2^{2+} (uranium in pink, oxygen in red) bound to DDD (gray ribbon) for every 1 ns of 100 ns MD trajectory (Na^+ and waters excluded from display). (**B**) Ball–and–stick drawing of the MD snapshot at t = 150 ns showing only the atoms in the vicinity of UO_2^{2+} (waters are excluded). Blue ribbon depicts DDD backbone and bases. (**C**) Local structure around uranium at t = 150 ns. Distances from central uranium are given in Å.

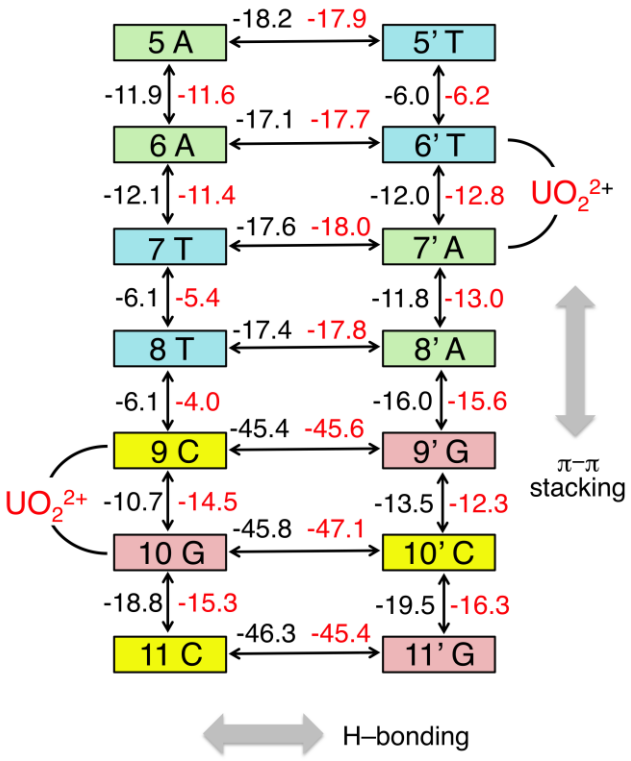

Figure 3. Average inter–fragment interaction energy (IFIE) amongst the nucleobases within d[CGCGAATTCGCG]$_2$ (DDD) with (red) and without (black) UO_2^{2+} obtained by fragment molecular orbital (FMO) calculations (unit in kcal/mol). Two UO_2^{2+} depicted in the figure are identical UO_2^{2+} which is crosslinking the two strands across the minor groove.